Petroleum Science
https://doi.org/10.1007/s12182-020-00456-8

ORIGINAL PAPER

Geochemical characteristics and genetic mechanism of the high-N_2 shale gas reservoir in the Longmaxi Formation, Dianqianbei Area, China

Ji-Lin Li[1,2] · Ting-Shan Zhang[1,2] · Yan-Jun Li[3] · Xing Liang[4] · Xin Wang[5] · Jie-Hui Zhang[4] · Zhao Zhang[4] · Hong-Lin Shu[4] · Da-Qian Rao[4]

Received: 5 June 2019

Abstract

As an important pilot target for shale gas exploration and development in China, the Longmaxi Formation shale in the Dianqianbei Area is characterized by high content of nitrogen, which severely increases exploration risk. Accordingly, this study explores the genesis of shale gas reservoir and the mechanism of nitrogen enrichment through investigating shale gas compositions, isotope features, and geochemical characteristics of associated gases. The high-nitrogen shale gas reservoir in the Longmaxi Formation is demonstrated to be a typical dry gas reservoir. Specifically, the alkane carbon isotope reversal is ascribed to the secondary cracking of crude oil and the Rayleigh fractionation induced by the basalt mantle plume. Such a thermogenic oil-type gas reservoir is composed of both oil-cracking gas and kerogen-cracking gas. The normally high nitrogen content (18.05%–40.92%) is attributed to organic matter cracking and thermal ammoniation in the high-maturity stage. Specifically, the high heat flow effect of the Emeishan mantle plume exacerbates the thermal cracking of organic matter in the Longmaxi Formation shale, accompanied by nitrogen generation. In comparison, the abnormally high nitrogen content (86.79%–98.54%) is ascribed to the communication between the atmosphere and deep underground fluids by deep faults, which results in hydrocarbon loss and nitrogen intrusion, acting as the key factor for deconstruction of the primary shale gas reservoir. Results of this study not only enrich research on genetic mechanism of high-maturity N_2 shale gas reservoirs, but also provide theoretical guidance for subsequent gas reservoir resource evaluation and well-drilling deployment in this area.

Keywords Longmaxi Formation · Shale gas reservoir · Isotope · High nitrogen content · Genetic mechanism

1 Introduction

Compared with conventional hydrocarbons, shale gas is essentially different in the occurrences, accumulation characteristics, and enrichment mechanisms under the low porosity and low permeability conditions (Wang and Li 2017; Wu et al. 2018; Chen et al. 2018a; Daniel 2018). Specifically, the Longmaxi Formation shale in the Dianqianbei Area is featured by over-high thermal maturity and high nitrogen content, which increases the difficulty and risk of shale gas exploration. Previous studies focus on the evaluation of shale gas richness from perspectives of sedimentary environment (Zhao et al. 2016; Deng et al. 2018), microscopic reservoir space (Hu et al. 2019; Wang et al. 2019) as well as reservoir-forming and diagenetic characteristics (Liu et al. 2013; Wang et al. 2015). In comparison, this study investigates the shale gas accumulation process in the Dianqianbei Area using geochemical

Edited by Jie Hao

✉ Ji-Lin Li
ljlgeology@163.com

✉ Ting-Shan Zhang
zts_3@126.com

1 School of Geoscience and Technology, Southwest Petroleum University, Chengdu 610500, Sichuan, China

2 State Key Laboratory of Oil and Gas Reservoir Geology and Exploitation, Chengdu 610500, Sichuan, China

3 ChuangYuan Oil and Gas Technology Development Co., Ltd, Chengdu 610500, Sichuan, China

4 PetroChina Zhejiang Oilfield Company, Hangzhou 310000, Zhejiang, China

5 PetroChina Huabei Oilfield Company, Renqiu 062550, Hebei, China

Published online: 06 May 2020

methods. Specifically, there are many key issues to be solved, including the genetic type of shale gas, the occurrence and enrichment law of shale gas, and the source of nitrogen in some high-nitrogen, low-carbon gas reservoirs. Elaboration of these issues will greatly promote the exploration and development process of shale gas in this area. It is generally easy to retain shale gas isotope distribution characteristics in the inherited simple basins such as Appalachian and Ordos Basins (Biryol et al. 2016; Feng et al. 2017), while it is much more difficult to reconstruct the shale gas isotope features in the foreland basins or multi-stage superimposed basins, such as the case in the Dianqianbei Area (Chen et al. 2018b), which makes it very challenging to distinguish shale gas genesis. Moreover, whether it is reliable to study high to over-high maturity shale gas using the traditional alkane isotope identification is still controversial (Feng et al. 2016; Liu et al. 2018). Recently, much attention has been paid to the high-nitrogen marine shale reservoirs in southern China (Guo and Liu 2013; Liu et al. 2016). As an important indicator to reflect preservation conditions of oil and gas reservoirs (Chen 2005; Jiao et al. 2017), nitrogen can also help identify shale gas source and components (Wang et al. 2018). However, too high nitrogen content will increase the exploration risk and affect the accuracy of subsequent gas reservoir evaluation and the reliability of the development plan. Existing research acknowledges many nitrogen sources, including atmosphere (Krooss et al. 1995), biodegradation (Baxby et al. 1994), thermal decomposition (Wellman et al. 1968), cracking of nitrogen-containing minerals (Jenden and Kaplan 1989), and crust or mantle (Krooss et al. 1995). So far, rare in-depth research has been conducted to explore the cause of the high nitrogen content in the shale gas reservoirs of the Dianqianbei Area.

Accordingly, this study investigates the rule of the multi-stage alkane isotope reversal in the high to over-high maturity shale gas through investigating the geochemical characteristics of the Longmaxi Formation shale gas, accompanied by establishment of a relatively stable non-hydrocarbon gas characteristic chart that can be used to clarify gas genesis. Moreover, through implementing thermal simulation experiments, this study quantitatively identifies proportions of various types of gas components with different sources. Furthermore, regional tectonics and thermal history are combined with the above results to systematically explore the cause of the "high nitrogen content and low hydrocarbon content" in some shale gas reservoirs. Finally, the genetic mechanism of the high maturity shale gas reservoir is elaborated, accompanied by construction of a model illustrating the shale gas accumulation process in the Dianqianbei Area. Results of this study are expected to provide an important geological basis for subsequent exploration and development of shale gas reservoirs in this area.

2 Geological setting

As a multi-stage superimposed basin developed on the Upper Yangtze platform, the Dianqianbei Depression is adjacent to the southern margin of the Sichuan Basin in the north, the Dianqian uplift in the south (Fig. 1), and the Diandongbei Depression in the west (Chen et al. 2018c). The depression is featured by strong tectonics in the south and west, and it is tectonically a typical slotted east–west extended fold belt composed of wide anticlines and closed synclines (Liang et al. 2011; He et al. 2019). As the main target layer for shale gas exploration, the Silurian Longmaxi Formation was deposited in the epicontinental sea environment bounded by paleouplifts and local highlands, which resulted from compression of the Middle and Upper Yangtze Block. Generally, the Silurian Longmaxi Formation is a set of deep-water organic-rich shale deposits formed in the constrained environment with depleted oxygen (Chen et al. 2018a; Li et al. 2019). This set of shale is about 200 m thick, with a TOC range of 0.19%–8.46% and a vitrinite reflectance (Ro) range of 2.2%–3.96%, which indicates high to over-high maturity that corresponds to the gas generation stage. The content of brittle minerals such as quartz and feldspar in shale is high, reaching 46%–84%. Large quantities of micropores and microfractures provide adsorption space and seepage channels during the shale gas accumulation (Wang 2017). Compared with geological features of large-scale commercial shale gas reservoirs such as those in fields of Barnett, Ohio, and Antrim in the USA (Fu et al. 2015; Zou et al. 2016; Jan et al. 2015), the Longmaxi Formation shale gas in the study area is of good resource basis and high exploration potential.

3 Samples and experimental methods

Shale gas samples were taken from four Longmaxi Formation shale gas industrial wells in the study area using high-pressure steel cylinders. Both the steel cylinders and the steel pipes can bear a pressure of 15 MPa. For high-pressure wells, samples were taken at the wellhead separator, and gas samples of about 5 MPa were filled in the cylinders after multiple replacements.

The shale gas composition analysis was completed at the Research Institute of Petroleum Exploration and Development. A MAT271 gas mass spectrometer was used to analyze the non-hydrocarbon components in the shale gas and the absolute contents of CH_4 and C_2H_6. The hydrocarbon gas was analyzed by a GC-9160 gas chromatograph, and the final data were normalized by mass

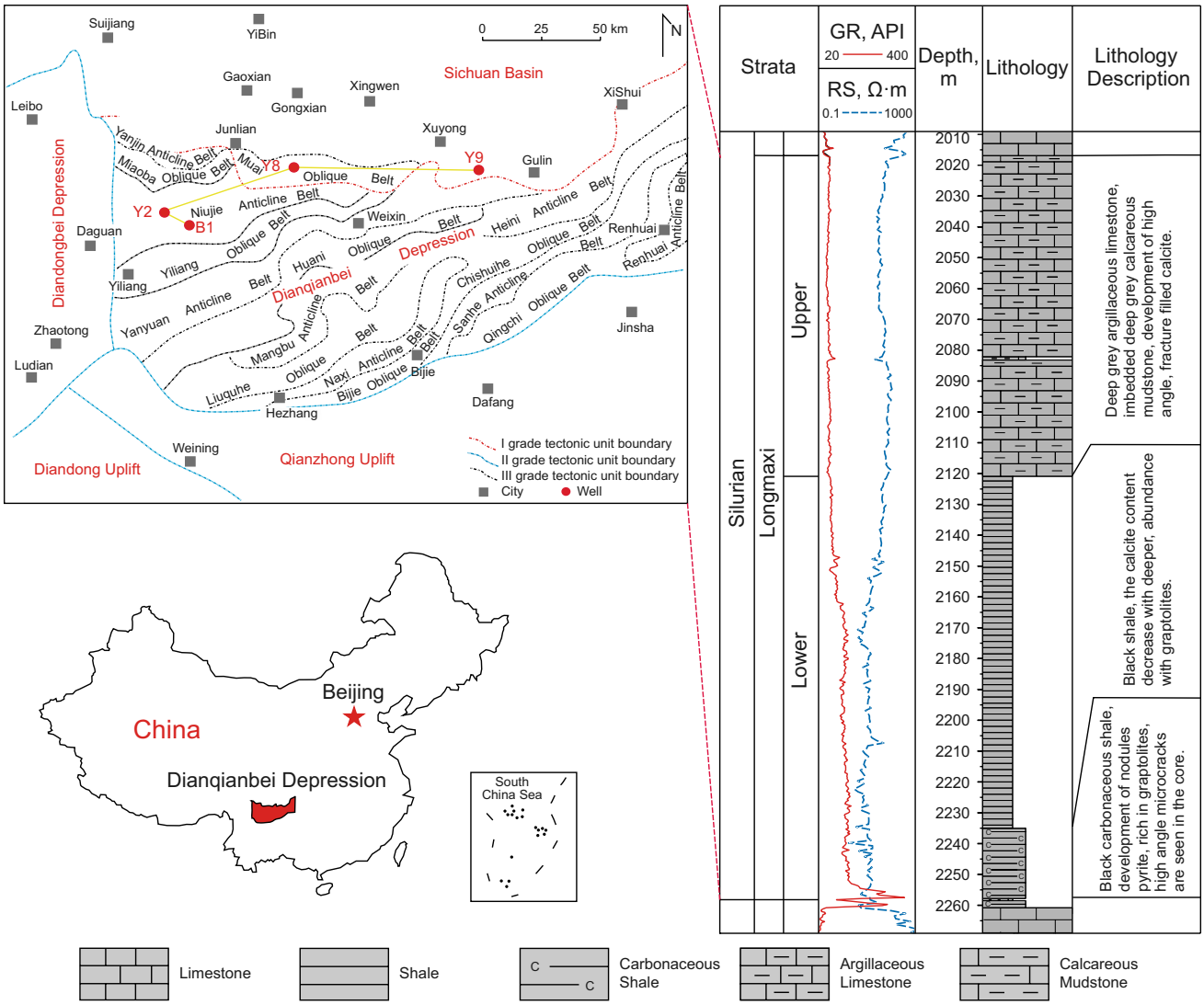

Fig. 1 Location of the study area and stratigraphic column

spectrometry and chromatographic data of CH_4, which has an analysis error of smaller than 0.5%. Determination of carbonate isotope was completed by first separating the gas components using an Agilent 6890 gas chromatograph, then oxidizing corresponding components to CO_2 in the high-temperature furnace, and finally obtaining the value by a Delta Plus XP mass spectrometer. Analysis errors of CH_4 and C_2H_6 were smaller than 0.5‰, and that of CO_2 was better than 1‰, with V-PDB as the calibration standard. Similarly, determination of hydrogen isotope involved separation of gas components by an Agilent 6890 gas chromatograph, reduction of components to H_2 in a high-temperature furnace, and acquisition of the hydrogen isotope by a MAT253 mass spectrometer. The analysis error was smaller than 0.5‰, and V-SMOW was used as the calibration standard. The helium isotope was analyzed by a Noblesse rare gas mass spectrometer, during which the two-stage separation system was employed for purification and enrichment. The $^3He/^4He$ analysis error was less than ± 1.5%. Nitrogen isotopes are measured on a MAT252 isotope mass spectrometer using the GC-C-MS method, which can achieve an accuracy of 0.5‰ with reference to V-AIR as the calibration standard.

4 Results and discussion

4.1 Shale gas compositions

According to experimental tests of the Longmaxi Formation shale samples from Wells Y2 and B1 (Table 1, Fig. 2a, b), the methane content greatly varies in the range of

Table 1 Shale gas compositions of typical exploration wells in the Dianqianbei Area

Sample no.	Formation	Depth, m	Gas components, %						C_1/C_{2+3}	Humidity coefficient C_{2+}/C_1, %
			CH_4	C_2H_6	C_3H_8	CO_2	N_2	Other		
Y2-01	S_1l	2734.27	0.13	0	0	8.95	90.87	0.05	–	0
Y2-02	S_1l	2740.74	1.29	0	0	8.62	90.02	0.07	–	0
Y2-03	S_1l	2745.47	1.06	0	0	6.46	92.37	0.11	–	0
Y2-04	S_1l	2749.54	2.5	0	0	6.34	91.03	0.13	–	0
Y2-05	S_1l	2751.94	8.02	0	0	5.13	86.79	0.06	–	0
Y2-06	S_1l	2755.19	2.01	0	0	3.1	94.87	0.02	–	0
Y2-07	S_1l	2758.6	2.66	0	0	5.35	91.91	0.08	–	0
Y2-08	S_1l	2760.81	0.52	0	0	1.06	98.39	0.03	–	0
Y2-09	S_1l	2763.74	0.53	0	0	1.52	97.9	0.05	–	0
Y2-10	S_1l	2767.73	0.48	0	0	0.92	98.54	0.06	–	0
B1-01	S_1l	2182.29	52.42	0.23	0.03	6.88	40.33	0.11	201.62	0.49
B1-02	S_1l	2193.83	79.15	0.31	0.01	1.8	18.57	0.16	247.34	0.40
B1-03	S_1l	2199.5	73.82	0.29	0.08	2.47	23.21	0.13	199.51	0.50
B1-04	S_1l	2213.79	59.58	0.23	0.62	5.23	34.21	0.13	70.09	1.41
B1-05	S_1l	2218.7	53.08	0.2	0.12	5.59	40.92	0.09	165.88	0.60
B1-06	S_1l	2231.35	77.23	0.21	0.12	2.03	20.18	0.23	234.03	0.43
B1-07	S_1l	2236.08	68.95	0.18	0.06	2.57	28.15	0.09	287.29	0.35
B1-08	S_1l	2246.1	80.09	0.26	0.01	1.49	18.05	0.1	296.63	0.34
B1-09	S_1l	2256.56	73.02	0.22	0.03	1.38	25.26	0.09	292.08	0.34
B1-10	S_1l	2260.06	72.23	0.2	0	2.61	24.89	0.07	361.15	0.28
B1-11	S_1l	2271.77	68.09	0.16	0	2.51	29.14	0.1	425.56	0.23
Y9-1	S_1l	2384	97.42	1.83	0.08	0.33	–	0.34	51.01	1.96
Y9-2	S_1l	2393	96.99	2.16	0.1	0	–	0.75	42.92	2.33
Y9-3	S_1l	2470	97.65	1.99	0.18	0.15	–	0.03	45.00	2.22
Y9-4	S_1l	2475	97.63	1.89	0.12	0.28	–	0.08	48.57	2.06
Y9-5	S_1l	2480	97.57	1.59	0.16	0.32	–	0.36	55.75	1.79
Y9-6	S_1l	2485	97.45	1.77	0.09	0	–	0.69	52.39	1.91
Y9-7	S_1l	2490	98.24	1.4	0.1	0.26	–	0	65.49	1.53
Y9-8	S_1l	2497	97.15	2.01	0.12	0.35	–	0.37	45.61	2.19
Y9-9	S_1l	2506	98.75	0.68	0.17	0.4	–	0	116.18	0.86
Y9-10	S_1l	2513	97.97	1.04	0.18	0.38	–	0.43	80.30	1.25
Y8-1	S_1l	2398	97.18	0.64	0	0.32	–	1.86	151.84	0.65
Y8-2	S_1l	2467	93.31	0.61	0.08	0.51	–	5.49	135.23	0.73
Y8-3	S_1l	2484	98.23	0.44	0	0.27	–	1.06	223.25	0.45
Y8-4	S_1l	2490	97.23	0.46	0	0	–	2.31	211.37	0.47
Y8-5	S_1l	2492	95.81	0.57	0.11	0.11	–	3.4	140.90	0.70
Y8-6	S_1l	2501	92.21	0	0.64	0.64	–	6.51	144.08	0.69
Y8-7	S_1l	2509	94.04	0.5	0	0.49	–	4.97	188.08	0.53

0.13%–98.75%. Except for Well Y2 that has high nitrogen content, all the other wells are seen with a small amount of ethane, with a content range from 0% to 2.16%, and only a few samples contain trace propane. The humidity coefficient (C_{2+}/C_1) is between 0.23% and 2.33%, with an average of 0.98%, which indicates typical dry gas reservoirs. The non-hydrocarbon gas is mainly CO_2 (0%–8.95%) and N_2 (18.05%–98.54%).

4.2 Isotope compositions and reversal characteristics of alkanes in the shale gas

The methane carbon isotope ($\delta^{13}C_1$) varies from $-27.9‰$ to $-20.8‰$, with an average of $-23.6‰$; the hydrogen isotope (δD) ranges from $-141‰$ to $-104‰$, with an average of $-129‰$; the ethane carbon isotope ($\delta^{13}C_2$) varies between $-31.8‰$ and $-29.3‰$, averaging $-30.8‰$; and

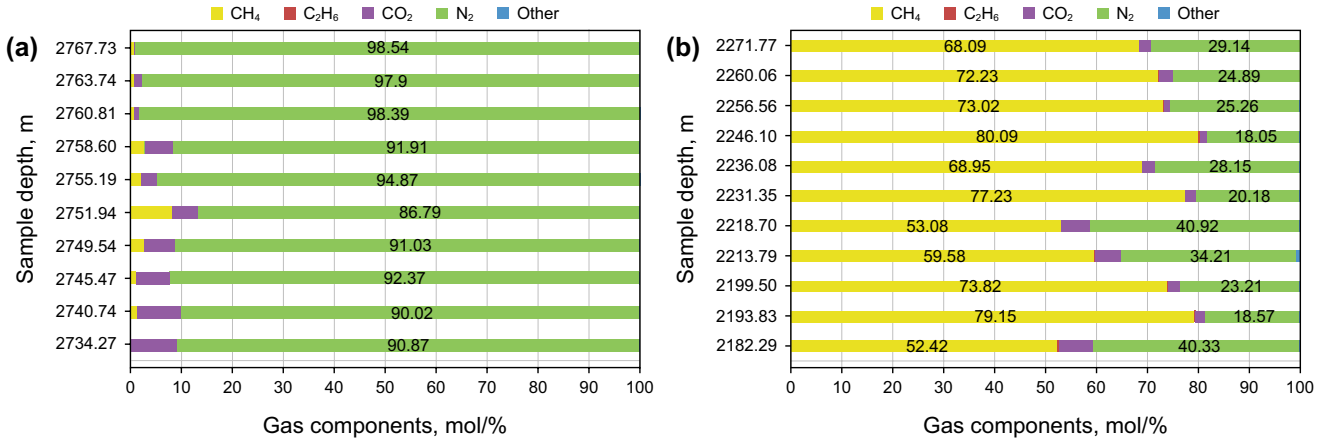

Fig. 2 Component contents of typical shale gas wells in Dianqianbei Area. **a** Sample in Well Y2; **b** Sample in Well B1

the propane carbon isotope ($\delta^{13}C_3$) ranges from −32.9‰ to −27.8‰, with an average of −29.3‰. Overall, $\delta^{13}C_1$ is much higher than $\delta^{13}C_2$, while $\delta^{13}C_2$ shares a similar range with $\delta^{13}C_3$ (Table 2).

Conventional natural gas is generally characterized by the monotonic positive sequence of carbon isotope. In comparison, the alkane isotope anomaly in shale gas is mainly reflected in the change of ethane carbon isotope ($\delta^{13}C_2$) with the increase in kerogen thermal maturity, presenting an anti-"S" shape curve. The $\delta^{13}C_2$ reversal that is defined by Tilley and Muehlenbachs (2013) refers to the phenomenon that $\delta^{13}C_2$ reaches the maximum at a reversal point, after which $\delta^{13}C_2$ starts to decrease. This reversal point is ascribed to the mixture of secondary cracking gas from liquid hydrocarbons with the pre-existing kerogen-cracking gas (Wu et al. 2015). A secondary reversal is defined at the moment that $\delta^{13}C_2$ becomes lighter than $\delta^{13}C_1$, which is speculated to be caused by excessively high thermal maturity

Table 2 Carbon and hydrogen isotopes of shale gas alkanes in typical exploration wells

Sample no.	Depth, m	$\delta^{13}C$(VPDB), ‰				δD(VSMOW), ‰
		CH_4	C_2H_6	C_3H_8	CO_2	CH_4
Y9	2384.00	−27.9	−29.3	−32.9	−13.9	−134
	2393.00	−24.3	−31.1	−32.5	–	−130
	2470.00	−25.9	−30.4	−27.8	−9.7	−133
	2475.00	−21.6	−30.6	−28.1	−8.3	−126
	2480.00	−20.8	−29.7	−28.7	−7.6	−114
	2485.00	−22.7	−31.3	–	–	−132
	2490.00	−23.6	−31.6	–	−8.1	−138
	2497.00	−24	−31.5	−28.8	−8.2	−133
	2506.00	−21.4	−30.5	−28	−5.1	−127
	2513.00	−23.5	−31.8	−28.2	−7.3	−129
Y8	2398.00	−21.6	−30.6		−8.3	−122
	2467.00	−20.8	−29.7	−28.7	−7.8	−104
	2484.00	−22.7	−31.3	–	−8.4	−130
	2490.00	−23.6	−31.6	–		−130
	2492.00	−24	−31.5	−28.8	−8.1	−128
	2501.00	−21.4	−30.5	−28	−6.2	−123
	2509.00	−23.5	−31.8	–	−6.9	−132
B1	2199.50	−30.7	–	–	–	−135
	2246.10	−31.8	–	–	–	−139
	2271.77	−30.8	–	–	–	−141

(Cao et al. 2015). Samples from representative Wells Y8 and Y9 are all in the reversal parts at the end of the anti-"S" shape curve. This is attributed to the cracking of heavy hydrocarbons and early-formed crude oil in the high to over-high maturity stage, which result in ethane with much larger volume and lighter isotopes than the contemporary ethane

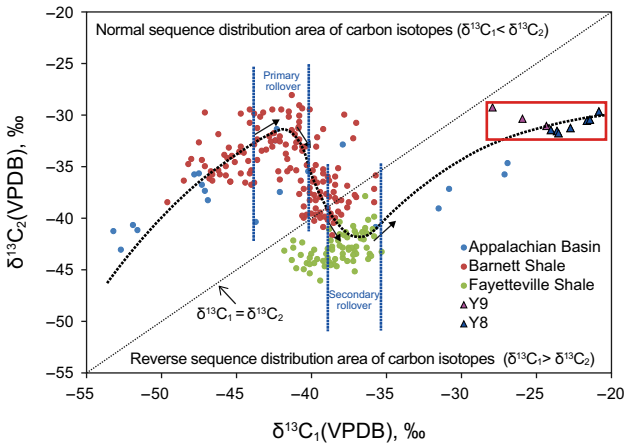

Fig. 3 Relationship between $\delta^{13}C_1$ and $\delta^{13}C_2$ of shale gas from North America Basin and Dianqianbei Area. Sample data of Appalachian Basin, Fortworth Basin, and Arkoma Basin come from references (Dai et al. 2014; Zumberge et al. 2012; Hill et al. 2007; Pashin et al. 2012)

(content less than 2%), leading to deconstruction of the positive carbon isotope sequence (Fig. 3). On the other hand, it is also ascribed to the Rayleigh fractionation effect, which occurs in the reduction reactions between mature ethane and formation water or iron-containing metals that are catalyzed by transition metals under high-temperature conditions (Michelsen et al. 2015) (Fig. 4). In the Middle and Late Permian, the Dianqianbei Area was affected by the thermal effect of the Emeishan basalt super mantle plume (Jiang et al. 2018; Wu et al. 2014), which led to the presence of many high-density methane inclusions in the Longmaxi Formation shale, with the homogenization temperature reaching 205 °C. Moreover, the overlain strata on the Longmaxi Formation shale are Silurian water-bearing clastic rocks, which also favor the occurrence of Rayleigh fractionation. In this process, a small amount of in situ $^{13}C_2H_6$ was involved in the reaction and converted into $^{13}CH_4$, which resulted in $^{13}C_2$ deficiency and $^{13}C_1$ enrichment, forming the carbon isotope reversal ($\delta^{13}C_1 > \delta^{13}C_2$). Moreover, such reversal was further enhanced by the thermochemical reaction of residual kerogen and formation water.

4.3 Genesis of gas hydrocarbons in the shale gas

The carbon isotope distribution in alkane gas is commonly used to identify sources of conventional gas and coalbed

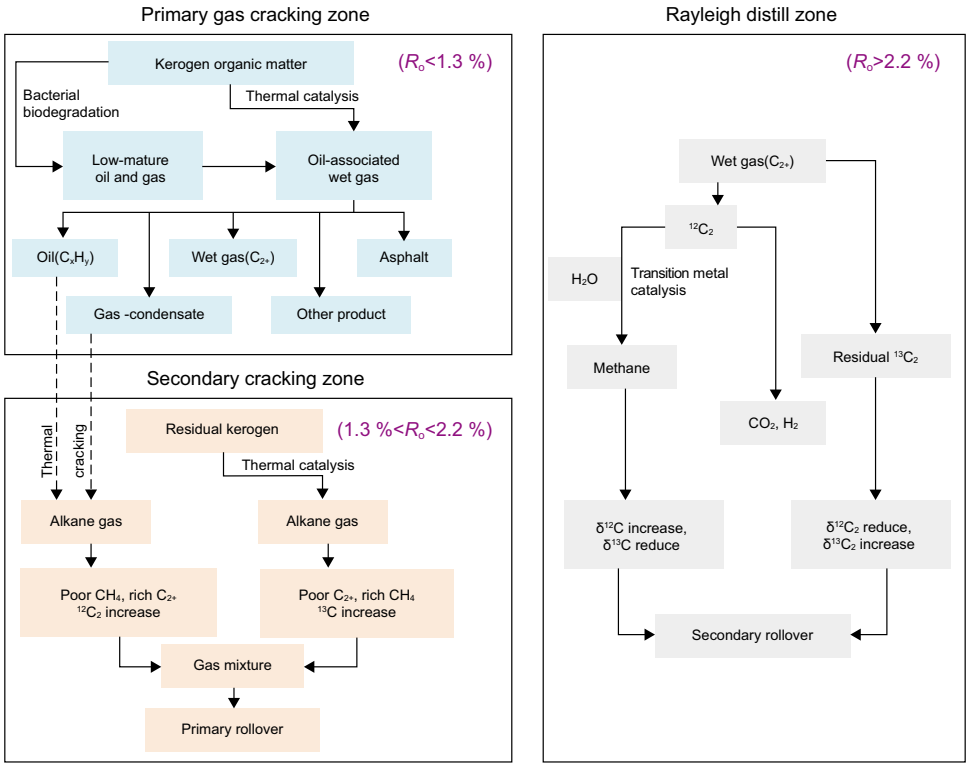

Fig. 4 Evolution process of carbon isotope in gas system with different maturity

methane, which has achieved good results in gas reservoir exploration practice. However, it is not applicable in the high to over-high maturity shale gas reservoirs where alkane carbon isotopic reversal is common. Many identification charts for conventional isotopes are not accurate any more. For instance, when classified using the detailed Bernard chart calibrated by conventional natural gas reservoir samples (Chen et al. 1995), the gas in the Dianqianbei Area falls into the coal-forming gas category and its mixed source area, which is contradictory to the fact that the gas originates from marine sapropel shales (Fig. 5a). Therefore, the Bernard series charts are almost ineffective for genesis identification of high to over-high maturity natural gas. Compared with shale gas in the North America, the Longmaxi Formation shale gas in the Dianqianbei Area has abnormal heavy $\delta^{13}C$ values and high $C_1/(C_2+C_3)$ ratios in the high to over-high maturity stage. As shown in Fig. 5b, samples from Wells Y9 and Y8 fall in the vicinity of the lower boundary of the thermogenic zone in the $\delta^{13}C(CO_2)$ and $\delta^{13}C(CH_4)$ cross-plot, which is related to the high thermal maturity of the alkane gas. Moreover, the average content of CO_2 is 2.28%, and the $\delta^{13}C(CO_2)$ is between $-10‰$ and $-8‰$, with an average of $-8.14‰$ (Table 2). Therefore, it can be inferred that CO_2 should mainly come from cracking of organic matter, with some mixed inorganic gas resulting from dissolution and cracking of carbonate minerals. According to migration of alkane isotopes in the kerogen cracking process, $\delta^{13}C(C_2H_6)$ is mainly controlled by kerogen type. The $\delta^{13}C(C_2H_6)$ value of the Longmaxi Formation shale

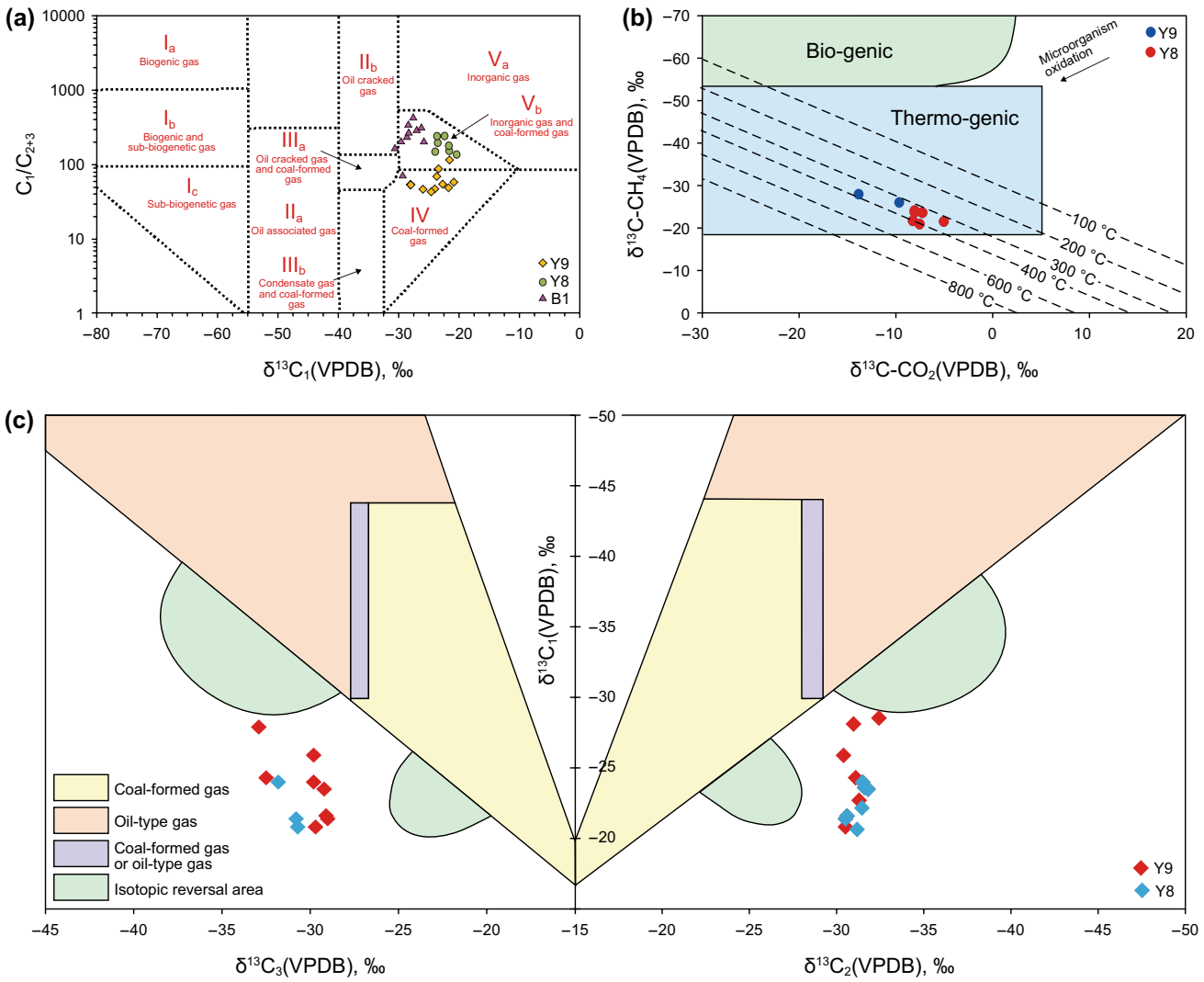

Fig. 5 Diagram for identification of genetic types of Longmaxi Formation shale gas components in the Dianqianbei Area. **a** Modified Bernard diagram about relationship between $\delta^{13}C$ and $C_1/(C_2+C_3)$, base map from reference (Chen et al. 1995); **b** relationship between $\delta^{13}C$-CO_2 and $\delta^{13}C$–CH_4, base map from reference (Kotarba 2001; Liu et al. 2016); **c** relationship between $\delta^{13}C_1$, $\delta^{13}C_2$, and $\delta^{13}C_3$, base map from reference (Dai et al. 2014; Liu et al. 2016)

gas in the study area is lower than − 28‰, which indicates sapropel-related oil-type gas. As shown in Fig. 5c, all the shale gas samples fall in the oil-type gas zone in the $\delta^{13}C_1$–$\delta^{13}C_2$–$\delta^{13}C_3$ gas source chart and are close to the isotope reversal zone. This is in line with above-stated results about the negative carbon isotope sequence of the secondary reversal, namely $\delta^{13}C_1 > \delta^{13}C_2 > \delta^{13}C_3$.

The unconventional carbon isotope partitioning of the Longmaxi Formation shale gas is partly caused by secondary cracking of pre-existing liquid hydrocarbons in the shale during the high maturity stage. According to thermal simulation results of the Longmaxi Formation kerogen and normal C_{22} alkane (crude oil equivalent) by the previous study (Qu et al. 2015), considering the fractionation mechanism of thermogenic gas isotope (Wei et al. 2015), linear trend models are, respectively, established for $\delta^{13}C_1$ and δD features of cracking products of crude oil and kerogen (Qu 2015) (Fig. 6).

$$\text{Crude oil-cracking gas: } \delta^{13}C = 0.1316\delta D - 22.405 \quad R^2 = 0.9087 \tag{1}$$

$$\text{Kerogen-cracking gas: } \delta^{13} = 0.1048\delta D - 6.269 \quad R^2 = 0.9190 \tag{2}$$

The two nearly parallel trend lines in the isotope cross-plot are located just in the vicinity of the upper and lower boundaries of the thermogenic area. A vertical line is drawn through the sample point, resulting in two intersection points with the two trend lines. These two points are used to, respectively, represent methane carbon isotope end values of cracking gas of crude oil and kerogen, denoted as $\delta^{13}C_{oil}$ and $\delta^{13}C_{kero}$, respectively. Assuming the proportion of oil-cracking gas is X, the methane carbon isotope of the mixture of two end members ($\delta^{13}C_{mix}$) can be expressed as follows:

$$\delta^{13}C_{mix} = X\delta^{13}C_{oil} + (1 - X)\delta^{13}C_{kero} \tag{3}$$

As shown in Table 3, the proportion of oil-cracking gas ranges between 9.32% and 28.90% for the Longmaxi Formation shale gas in the study area, with an average of 16.7%. As the thermal maturity increases to 2.0%, early-formed heavy hydrocarbons are fully cracked, contributing to the largest proportion of oil-cracking gas. With further increased maturity, wet components in the oil-cracking gas are continuously cracked, and no massive oil-cracking gas is formed, which result in the decreasing proportion of oil-cracking gas.

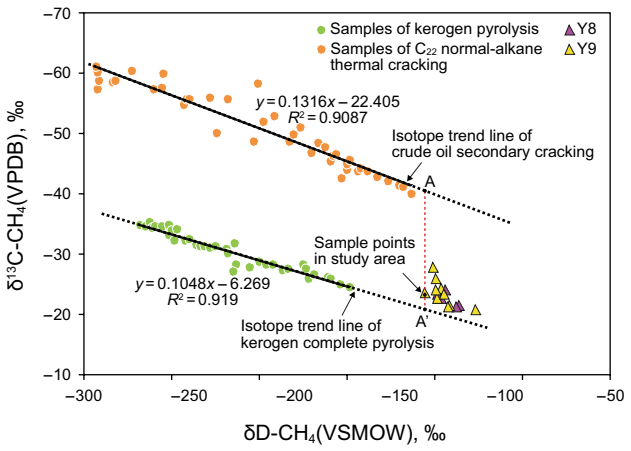

Fig. 6 Relationship between methane carbon and hydrogen isotopes and distinguishing model of mixed gas components (Qu 2015). (Thermal simulation results of kerogen and C_{22} are from Qu et al. 2015.)

4.4 Genesis of high-content nitrogen

It is critical to investigate genesis and enrichment of N_2 in shale gas reservoirs so as to better understand hydrocarbon generation processes and hydrocarbon resource potentials of mature shale. Moreover, it has practical significance for predicting gas components in gas reservoirs and reducing exploration risks. In terms of gas components in the shale gas reservoirs of the study area, N_2 and CH_4 are dominant in most samples, with a few alkanes, rare gases, and CO_2. As demonstrated in isotopic experiments, $\delta^{15}N$ in the shale gas reservoir of the Dianqianbei Area greatly varies between − 2.09‰ and 7.65‰ (Table 4), and such large variation range suggests highly diversified types of N_2 genesis.

The conventional high nitrogen gas reservoir in Well B1 is representative of a certain type of gas reservoir, with the N_2 content ranging between 18.05% and 40.92% (averaging 27.54%). As shown in the $\delta^{15}N$–N_2 cross-plot (Fig. 7a), most samples from Well B1 have a $\delta^{15}N$ range of 4‰–8‰, with an average of 4.77‰. According to the experimental thermal simulation results, N_2 resulting from organic matter cracking generally has a $\delta^{15}N$ range between 4‰ and 20‰, which becomes heavier as the maturity increases (Kotarba and Lewan 2013). Therefore, it can be preliminarily inferred that the high N_2 content in the gas reservoir of Well B1 is mainly ascribed to organic matter cracking. According to the $\delta^{15}N$–$\delta^{13}C_1$ cross-plot (Fig. 7b), the $\delta^{13}C_1$ value is between − 30.5‰ and − 25.8‰. As the $\delta^{13}C_1$ value grows, $\delta^{15}N$ becomes heavier, presenting features of organic matter cracking during the high to over-high maturity stage.

During the Permian (about 259 Ma ago), the Southwestern Sichuan Region experienced the Emeishan basalt eruption event, and the Dianqianbei Area was in the middle to outer zone of the Emeishan mantle plume (Fig. 8), which provided thermodynamics for maturation of the Longmaxi Formation source rocks. In order to evaluate the influence of the mantle plume on the regionally differential thermal

Table 3 Evaluation results of shale gas component proportions in Wells Y9 and Y8 of the Dianqianbei Area

Well	Sample depth, m	$\delta^{13}C_{mix}$ (VPDB), ‰	δD (VSMOW), ‰	Oil-cracked gas $\delta^{13}C_{oil}$, ‰	Kerogen pyrolysis gas $\delta^{13}C_{kero}$, ‰	Ratio of oil-cracked gas, %
Y9	2393.00	−24.3	−130	−39.5	−19.9	22.46
	2470.00	−25.9	−133	−39.9	−20.2	28.90
	2475.00	−21.6	−126	−39.0	−19.5	10.90
	2480.00	−20.8	−114	−37.4	−18.2	13.46
	2485.00	−22.7	−132	−39.8	−20.1	13.20
	2490.00	−23.6	−138	−40.6	−20.7	14.46
	2497.00	−24	−133	−39.9	−20.2	19.25
	2506.00	−21.4	−127	−39.1	−19.6	9.32
	2513.00	−23.5	−129	−39.4	−19.8	18.94
Y8	2398.74	−21.6	−122	−38.5	−19.1	13.12
	2467.00	−20.8	−104	−36.1	−17.2	19.19
	2484.53	−22.7	−130	−39.5	−19.9	14.31
	2488.25	−23.6	−130	−39.5	−19.9	18.89
	2492.63	−24	−128	−39.2	−19.7	22.06
	2501.27	−21.4	−123	−38.6	−19.2	11.53
	2509.61	−23.5	−132	−39.8	−20.1	17.27

Table 4 Isotopic characteristics of nitrogen and methane carbon in Wells Y2 and B1 of the Dianqianbei Area

Sample no.	Depth, m	Gas components, %		Isotopic content	
		CH_4	N_2	$\delta^{13}C(CH_4)$(VPDB), ‰	$\delta^{15}N$(VAIR), ‰
Y2	2734.27	0.13	90.87	−32.1	−0.47
	2740.74	1.29	90.02	−33.5	−1.03
	2745.47	1.06	92.37	−34.6	0.23
	2749.54	2.5	91.03	−36.7	−1.45
	2751.94	8.02	86.79	−35.1	−2.09
	2755.19	2.01	94.87	−31.6	−0.49
	2758.6	2.66	91.91	−30.2	−0.12
	2760.81	0.52	98.39	−29.5	0.79
	2763.74	0.53	97.9	−30.8	0.35
	2767.73	0.48	98.54	−33.4	−0.67
B1	2182.29	52.42	40.33	−29.6	1.73
	2193.83	79.15	18.57	−28.4	7.65
	2199.5	73.82	23.21	−25.8	6.23
	2213.79	59.58	34.21	−29.2	2.23
	2218.7	53.08	40.92	−30.5	−0.46
	2231.35	77.23	20.18	−28.6	5.76
	2236.08	68.95	28.15	−27.4	4.39
	2246.1	80.09	18.05	−26.1	6.87
	2256.56	73.02	25.26	−27.1	5.66
	2260.06	72.23	24.89	−28.3	5.57
	2271.77	68.09	29.14	−27.8	6.89

evolution of source rocks, two typical wells located in different zones are selected, namely the Well H1 near the middle zone of the mantle plume and the Well CY84 outside the mantle plume zone. Subsequently, thermal evolution of source rocks is correlated with the burial depth (Fig. 9). Compared with source rocks in Well CY84 that experienced

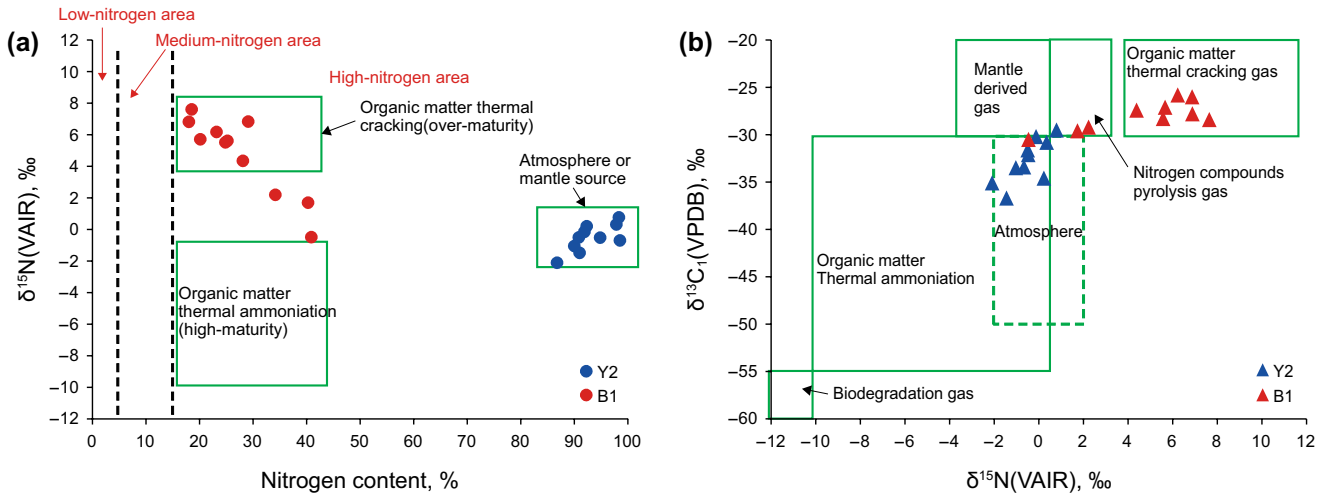

Fig. 7 Diagram to identify N_2 genesis of Longmaxi Formation shale gas in Dianqianbei Area. **a** Relationship between $\delta^{15}N$ and nitrogen content. Base chart comes from reference (Zhu et al. 2000; Chen et al. 2001). **b** Relationship between $\delta^{13}C_1$ and $\delta^{15}N$. Base chart comes from reference (Li et al. 2013; Jiao et al. 2017; Xia et al. 2018)

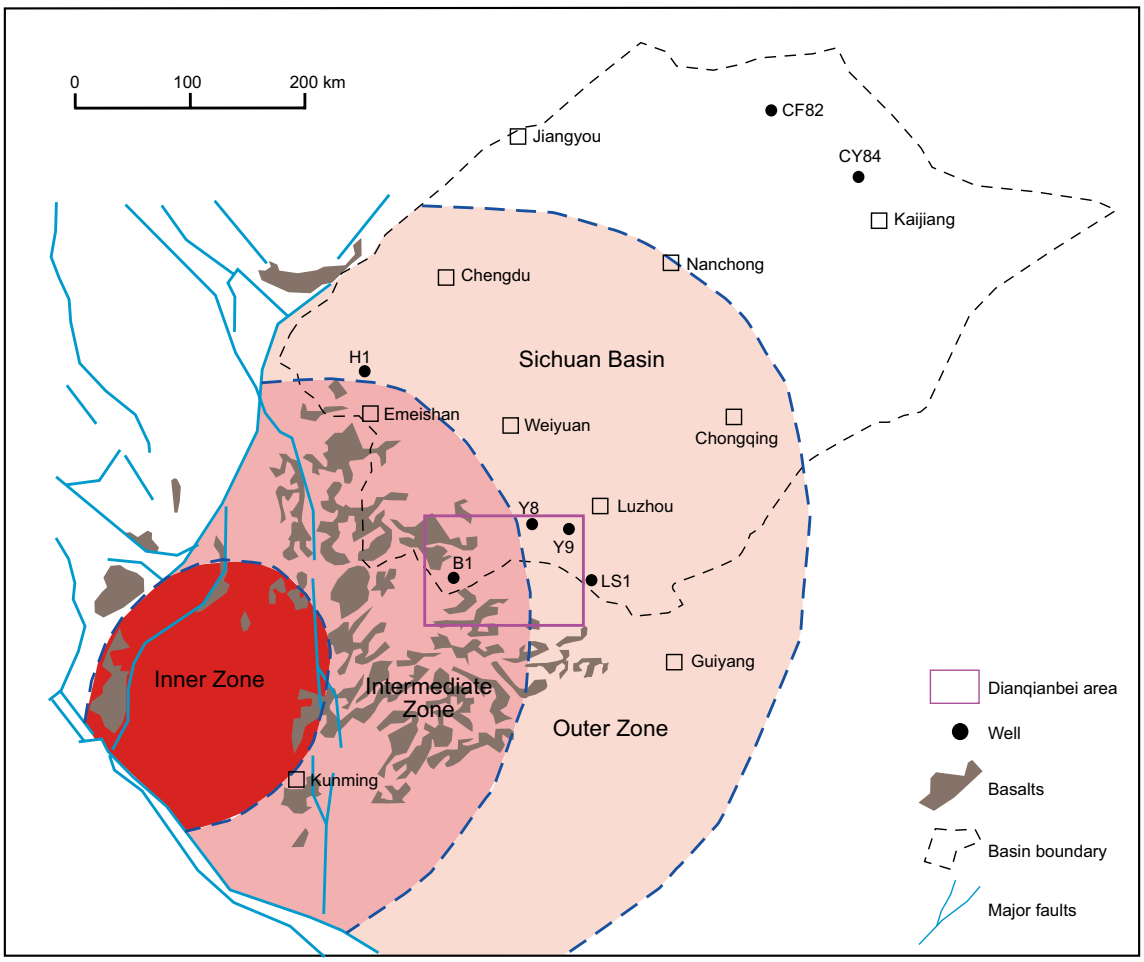

Fig. 8 Geology of the Emeishan large igneous province and the boreholes in Dianqianbei Area. Base map modified from reference (Xu et al. 2004)

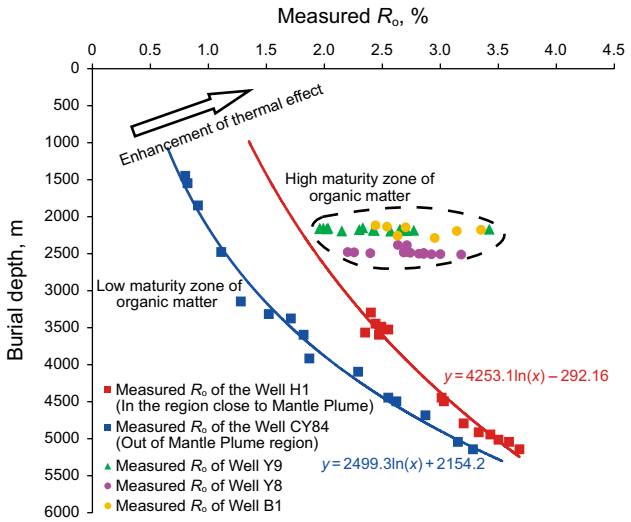

Fig. 9 Measured R_o values of the representative wells around Emeishan mantle plume. R_o values of Well H1 and CY84 come from reference (Zhu et al. 2010)

normal thermal evolution, those in Well H1 underwent ultra-high temperature caused by the mantle plume thermal activity in a short period of time, reflected in the rightward jumping of the actual maturity measurement from the normal trend line. Maturities of shales in Wells Y9, Y8, and B1 are between 1.96% and 3.42%, which are higher than those in the normal burial conditions. During the overmature stage ($R_o > 2\%$), organic matter is affected by the heat flow of the mantle plume, which results in full cracking and denitrification, accompanied by generation of massive N_2. Moreover, the thermal evolution history of the Longmaxi Formation source rocks is established (Fig. 10) (Rao et al. 2013), according to the T-t thermal history path and the chemical kinetic model (Easy $\%R_o$). Specifically, the Well CF82 in the Northern Sichuan Area is far from the mantle plume-affected zone, and thus Silurian source rocks there are characterized by gradual and continuous thermal evolution, becoming mature at the end of the Permian and finalized in the Cretaceous, with the highest paleotemperature of 180 °C. In comparison, the Well LS1 in the Southern Sichuan Area is located in the middle of the mantle plume-affected zone, and Silurian source rocks there were immature during the Caledonian period, but quickly entered the overmature stage during the Permian due to the anomalous thermal effect of the mantle plume, which resulted in a sharp temperature increase of 250 °C and a short oil window of only 15 Ma. The maturity of Silurian source rocks in the Well LS1 finally reached 3.1% in the Late Permian. Well B1 shares similar thermal history evolution with Well LS1, and source rocks there were quickly heated to be more than 300 °C during the Late Permian, meeting the chemical kinetic conditions of organic matter cracking and high N_2 production (Littke et al. 1995).

A few samples from Well B1 fall out of the thermal cracking genesis in the identification chart. However, they are less likely to originate from volcanic activity and the deep part of the upper mantle or from thermal cracking of nitrogen-containing clay minerals. The $^3He/^4He$ ratio of the Longmaxi Formation shale is between 1.86×10^{-8} and 3.96×10^{-8} (equivalent to R/Ra ratio of 0.01–0.03), which is much lower than the critical condition of mantle-originated helium ($R/Ra > 0.1$). Moreover, NH_4^+ ions in nitrogen-rich clay minerals are of strong thermal stability, which can only be decomposed when the temperature exceeds 1000 °C (Whelan et al. 1988). In that case, generated N_2 needs to survive the differentiation process during migration, before it can be accumulated as the high-N_2 reservoir. Therefore, it can be concluded that the high-nitrogen Longmaxi Formation shale reservoir in the study area is not a product of inorganic mineral thermal cracking. In this study, it is considered to be related to thermal ammoniation in the high maturity stage of organic matter. When the activation energy required for the amino group ($-NH_2$) is met, NH_3 is produced, which subsequently reacts with CO_2 and Fe_2O_3, generating N_2 with a $\delta^{15}N$ range of $-10‰$ to $-1‰$. Meanwhile, the associated methane has a $\delta^{13}C$ range of $-55‰$ to $-30‰$. These features are consistent with the trend line in the $\delta^{15}N$–$\delta^{13}C$ cross-plot

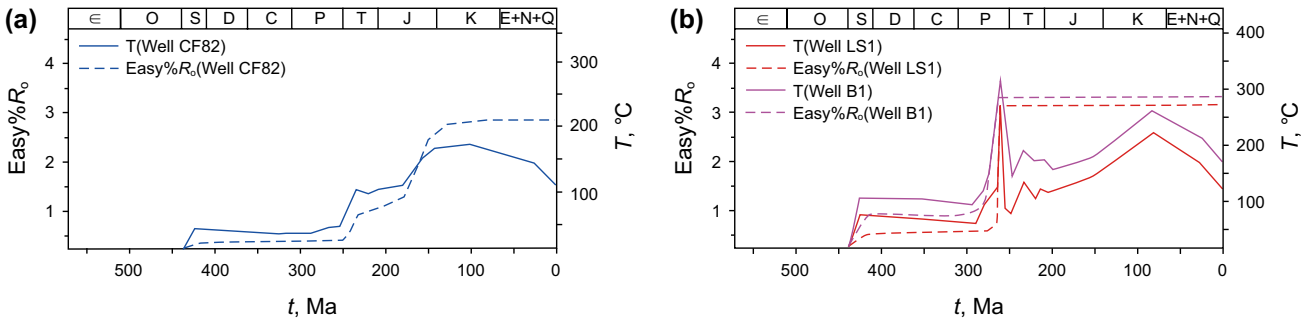

Fig. 10 Temperature and maturity evolution history of Silurian source rock of the representative boreholes. Sample data of Well CF82 and LS1 come from reference (Rao et al. 2013)

(Fig. 7b). To conclude, the high content of nitrogen in the shale gas reservoir of Well B1 is mainly ascribed to thermal cracking of organic matter and partly to thermal amination.

The abnormally high nitrogen gas reservoir in Well Y2 is representative of another type of gas reservoir, with the N_2 content ranging between 86.79% and 98.54% (averaging 93.27%) and the $\delta^{15}N$ value between −2.09‰ and 0.79‰ (Fig. 7a). These features are basically consistent with geochemical characteristics of the atmospheric N_2 ($\delta^{15}N \approx 0$). Through investigation into tectonic deformation in the Dianqianbei Area, it is found that the Indosinian movement in the Middle and Late Triassic is accompanied by strong tectonic compression that results in a series of massively deformed tightly closed fault belts. Specifically, located at the west flank of the Niujie Anticline in the Dianqianbei Area, the Well Y2 is at the flank of the gentle anticline, where inherited active deep faults are present. These faults enhance the circulation between atmospheric leaching water on the ground surface and fluids deep in the subsurface, adversely affecting preservation of early formed shale gas reservoirs. In addition, those main faults that cut through the basement are associated with derivative secondary faults, forming densely distributed fault belts that subsequently act as primary channels for hydrocarbon gas loss and external fluid intrusion. The alkane gas in the Lower Triassic shale gas reservoirs gets washed multiple times and finally releases along those deep faults to the surface. In this context, methane with heavier $\delta^{13}C$ is more soluble in water and thus preferentially washed away, leading to light $\delta^{13}C$ signatures (−36.7‰ to −29.5‰) of methane in the shale gas reservoir (Fig. 7b). Meanwhile, the downward infiltrating atmospheric water enters the gas reservoir with carried N_2, resulting in a relative large proportion of atmospheric N_2 and a relative small proportion of thermogenic N_2 as observed in Well Y2.

4.5 Shale gas formation mechanism

There are mainly three episodes of tectonic movements after the deposition of the Lower Silurian Longmaxi Formation shale in the study area, namely the Caledonian, the Hercynian-Indosinian-Yanshanian, and the Sichuan-Himalayan. During the Caledonian, marine organic-rich shale rapidly subsided, accompanied by gradually growing maturity. During the immature stage ($R_o < 0.55\%$), organic matter was decomposed by microbes to form a small amount of biogas. Then, the source rocks entered the low maturity stage ($0.55\% < R_o < 0.7\%$) and thus the hydrocarbon generation threshold during the Late Caledonian (420 Ma), associated with oil generation. The hydrocarbon generation process was intermittently interrupted by the Hercynian uplifting. Then, source rocks entered the oil window in the Late Hercynian (280 Ma ago), which was accompanied by generation of massive CO_2 in addition to liquid hydrocarbons. At the end of the Hercynian during the Middle and Late Permian, the Emeishan basalt erupted. The continuous, rapid burial and the high anomalous heat flow of basalt magma exacerbated the maturation of hydrocarbon-generating organic matter, contributing to significantly earlier (90–110 Ma) occurrence of hydrocarbon generation peaks. Moreover, the greatly shortened oil window was followed by an extended gas formation process. In the early stage of the Indosinian Movement, organic matter entered into a high maturity stage ($R_o > 1.3\%$), associated with thermal cracking of residual kerogen and liquid hydrocarbons to wet gas, gradually decreasing CO_2 yield, and generation of a small amount of N_2 by thermal ammoniation. During this period, the $\delta^{13}C_1$ value was relatively stable. With formation of more and more oil-cracking gas, more light $\delta^{13}C$ ethane was generated, and carbon isotope reversal occurred when R_o reached 1.8%. In the middle of the Indosinian, all heavy hydrocarbon components such as crude oil were cracked into gaseous hydrocarbons, and wet gas started to crack when R_o reached 2.0%. During the Yanshanian, the study area was in a stable subsidence stage, when the carbon isotope reversal reached the maximum. At that time, wet gas was cracked in a large amount, and the yield of organic matter cracking-related nitrogen gradually increased, approaching 50% of the hydrocarbon generation rate. Influenced by both the long-term subsidence and thus deep burial as well as the regional basalt mantle plume, the Longmaxi Formation shale reached the temperature conditions required for Rayleigh fractionation, accompanied by partial conversion of $^{13}C_2H_6$ to $^{13}CH_4$ and maintained carbon isotope reversal. Subsequently, during the Sichuan-Himalayan tectonic cycles, stably distributed Longmaxi Formation shale becomes elevated due to rapid uplifting. Moreover, junctions of anticlines and synclines in the strongly compressed fold bet are subjected to development of deep faults. Furthermore, the flank of an anticline is vulnerable to tectonic uplift and denudation. All these factors result in poor sealing and storage conditions in the peripheries of deep faults and the tops of shallow buried anticlines, leading to loss of early-formed hydrocarbon gas and intrusion of atmospheric gas (Fig. 11).

In this study, it is suggested to first locate relatively low-maturity shale gas targets in the Longmaxi Formation of the study area. Moreover, the central and northern parts of the study area, where tectonics are weak and deep faults are absent, are favorable for shale gas enrichment, and thus drilling risk of meeting low-abundance, high-nitrogen shale gas reservoir is effectively reduced there.

5 Conclusions

The high-nitrogen shale gas reservoir of the Longmaxi Formation in the Dianqianbei Area is a typical dry gas reservoir. The complete carbon isotope reversal ($\delta^{13}C_1 > \delta^{13}C_2$)

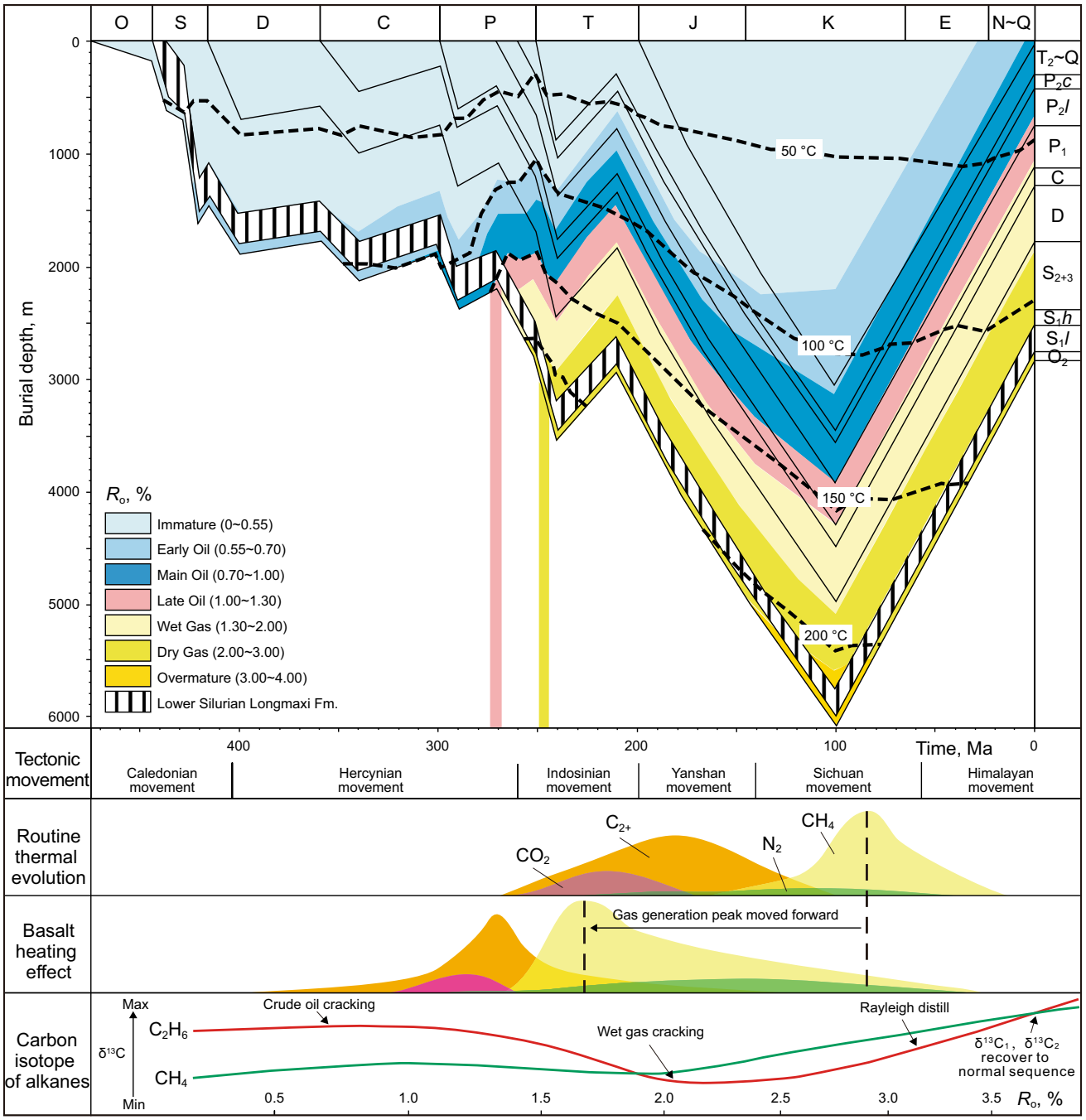

Fig. 11 Thermal history and evolution model of Longmaxi Formation shale gas in Dianqianbei Area

is speculated to result from the secondary cracking of early-formed liquid hydrocarbons in the high to over-high maturity stage as well as the high-temperature Rayleigh fractionation induced by the mantle plume heat flow. According to isotope migration features of alkanes and CO_2, the Longmaxi Formation shale gas is identified as a type of sapropel-related thermogenic oil-type gas. Through application of the thermal simulation model of crude oil and kerogen, proportions of various types of gases in the shale gas are determined. As the thermal maturity increases, the proportion of oil-cracking gas first increases and then decreases. As for the normally high nitrogen content (18.05%–40.92%), it is believed to result from organic matter thermal cracking and thermal ammoniation in the high-maturity stage. Specifically, the high heat flow effect of the Emeishan mantle plume exacerbates the thermal cracking of organic matter in the Longmaxi Formation shale, accompanied by nitrogen generation. In comparison, the abnormally high nitrogen

content (86.79%–98.54%) is ascribed to the communication between the atmosphere and deep underground fluids by deep faults, which results in hydrocarbon loss and nitrogen intrusion. Influenced by the basalt mantle plume, the shale gas accumulation process is featured by accelerated organic matter maturation, much earlier (90–110 Ma) arrival of the hydrocarbon generation peak, entrance into the wet gas generation stage and subsequent cracking stage during the Early Indosinian, and occurrence of carbon isotope reversal during the Yanshanian continuous subsidence.

Acknowledgements This research was financially supported by the National Science and Technology Major Project (2017ZX05063002–009), National Natural Science Foundation of China (41772150), Sichuan Province's Key Project of Research and Development (18ZDYF0884), Qian Ke He Platform Talents [2017]5789-16.

References

Baxby M, Patience RL, Bartle KD. The origin and diagenesis of sedimentary organic nitrogen. J Pet Geol. 1994;17(2):211–30. https://doi.org/10.1111/j.1747-5457.1994.tb00127.x.

Biryol CB, Wagner LS, Fischer KM, et al. Relationship between observed upper mantle structures and recent tectonic activity across the Southeastern United States. J Geophys Res Solid Earth. 2016;121(5):3393–414. https://doi.org/10.1002/2015JB012698.

Cao CH, Tang QY, Zhang MJ, et al. Carbon isotope reversals of Changning-Weiyuan region shale gas, Sichuan Basin. Acta Geol Sin (English Edition). 2015;89(s1):375–7.

Chen AD. Nitrogen as an index of oil–gas preservation conditions in marine strata. Pet Geol Exp. 2005;01:85–9 **(in Chinese)**.

Chen HH, Sun YC, Sun QM. Application of the δ^{13} rayleigh fractional model to determine the processes of gas migration and accumulation. Pet Explor Dev. 1995;22(2):29–33 **(in Chinese)**.

Chen CP, Mei BW, Zhu CS. Nitrogen isotopic composition and distribution of natural gases in Tarim basin. Geology-Geochemistry. 2001;29(4):46–9 **(in Chinese)**.

Chen XH, Liu ZC, Liang X, et al. The shale gas revolution in China—problems and countermeasures. Earth Sci Res J. 2018a;22(3):215–21. https://doi.org/10.15446/esrj.v22n3.74390.

Chen ZX, Lei YL, Hu Y, et al. Structural analysis of multi-level detachments and identification of deep-seated anticline. Pet Explor Dev. 2018b;45(2):281–9. https://doi.org/10.1016/S1876-3804(18)30031-4.

Chen KL, Zhang TS, Chen XH, et al. Model construction of micro-pores in shale: a case study of Silurian Longmaxi Formation shale in Dianqianbei area, SW China. Pet Explor Dev. 2018c;45(3):412–21. https://doi.org/10.1016/S1876-3804(18)30046-6.

Dai JX, Zou CN, Liao SM, et al. Geochemistry of the extremely high thermal maturity Longmaxi shale gas, southern Sichuan Basin. Organ Geochem. 2014;74:3–12. https://doi.org/10.1016/j.orggeochem.2014.01.018.

Daniel JS. The successful development of gas and oil resources from shales in North America. J Pet Sci Eng. 2018;163:399–420. https://doi.org/10.1016/j.petrol.2017.12.084.

Deng X, Kang ZH, Chen YY, et al. Sedimentary environment and reservoir characteristics of Longmaxi Formation shale in Sichuan Chongqing and Hubei area. J Northeast Pet Univ. 2018;42(2):80–7 **(in Chinese)**.

Feng ZQ, Liu D, Huang SP, et al. Carbon isotopic composition of shale gas in the Silurian Longmaxi Formation of the Changning area, Sichuan Basin. Pet Explor Dev. 2016;43(5):769–77. https://doi.org/10.1016/S1876-3804(16)30092-1.

Feng M, An MJ, Dong S. Tectonic history of the ordos block and Qinling Orogen inferred from crustal thickness. Geophys J Int. 2017;210(1):303–20. https://doi.org/10.1093/gji/ggx163.

Fu QL, Horvath SC, Potter EC, et al. Log-derived thickness and porosity of the Barnett Shale, Fort Worth basin, Texas: implications for assessment of gas shale resources. AAPG Bull. 2015;99(1):119–41. https://doi.org/10.1306/07171413018.

Guo TL, Liu RB. Implications from marine shale gas exploration breakthrough in complicated structural area at high thermal stage: taking Longmaxi Formation in Well JY1 as an example. Nat Gas Geosci. 2013;24(04):643–51 **(in Chinese)**.

He DF, Lu RQ, Huang HY, et al. Tectonic and geological setting of the earthquake hazards in the Changning shale gas development zone, Sichuan Basin, SW China. Pet Explor Dev. 2019;46(5):1051–64. https://doi.org/10.1016/S1876-3804(19)60262-4.

Hill RJ, Jarvie DM, Zumberge J, et al. Oil and gas geochemistry and petroleum systems of the Fort Worth Basin. AAPG Bull. 2007;91(4):445–73. https://doi.org/10.1306/11030606014.

Hu HY, Hao F, Guo XS, et al. Effect of lithofacies on the pore system of over-mature Longmaxi shale in the Jiaoshiba area, Sichuan Basin, China. Mar Pet Geol. 2019;109:886–98. https://doi.org/10.1016/j.marpetgeo.2019.06.050.

Jan TH, Mart Z, Susanne N, et al. Sweet spot identification in underexplored shales using multidisciplinary reservoir characterization and key performance indicators: example of the Posidonia Shale Formation in the Netherlands. J Nat Gas Sci Eng. 2015;27:558–77. https://doi.org/10.1016/j.jngse.2015.08.032.

Jenden PD, Kaplan IR. Origin of natural gas in Sacramento basin, California. AAPG Bull. 1989;73(4):431–53. https://doi.org/10.1306/44b49fc9-170a-11d7-8645000102c1865d.

Jiang Q, Qiu NS, Zhu CQ. Heat flow study of the Emeishan large igneous province region: implications for the geodynamics of the Emeishan mantle plume. Tectonophysics. 2018;724–725:11–27. https://doi.org/10.1016/j.tecto.2017.12.027.

Jiao WW, Wang SX, Cheng LJ, et al. The reason of high nitrogen content and low hydrocarbon content of shale gas from the Lower Cambrian Niutitang Formation in southeast Chongqing. Nat Gas Geosci. 2017;28(12):1882–90 **(in Chinese)**.

Kotarba MJ. Composition and origin of coalbed gases in the Upper Silesian and Lublin Basins, Poland. Organ Geochem. 2001;32(1):163–80. https://doi.org/10.1016/S0146-6380(00)00134-0.

Kotarba MJ, Lewan MD. Sources of natural gases in Middle Cambrian reservoirs in Polish and Lithuanian Baltic Basin as determined by stable isotopes and hydrous pyrolysis of Lower Palaeozoic source rocks. Chem Geol. 2013;345:62–76. https://doi.org/10.1016/j.chemgeo.2013.02.023.

Krooss BM, Littke R, Müller B, et al. Generation of nitrogen and methane from sedimentary organic matter: implications on the dynamic

of natural gas accumulations. Chem Geol. 1995;126(3–4):291–318. https://doi.org/10.1016/0009-2541(95)00124-7.
Li J, Li ZS, Wang DL, et al. Geochemical characteristics and N2 source of nitrogen riched natural gas in Tarim Basin. Acta Pet Sin. 2013;34(S1):102–11 **(in Chinese)**.
Li JL, Zhang TS, Liang X, et al. Relation and contribution rate of graptolite to organic matter enrichment in shale: a case study from Well YS118 at the southern margin of the Sichuan Basin. Nat Gas Ind. 2019;39(12):40–4 **(in Chinese)**.
Liang X, Ye X, Zhang JH, et al. Reservoir forming conditions and favorable exploration zones of shale gas in the Weixin Sag, Dianqianbei Depression. Pet Explor Dev. 2011;38(6):693–9 **(in Chinese)**.
Littke R, Krooss B, Idiz E, et al. Molecular nitrogen in natural gas accumulation: generation from sedimentary organic matter at high temperatures. AAPG Bull. 1995;79(3):410–30. https://doi.org/10.1016/0140-6701(95)95070-2.
Liu SG, Ma WX, Jansa L, et al. Characteristics of the shale gas reservoir rocks in the Lower Silurian Longmaxi Formation, East Sichuan Basin, China. Energy Explor Exploit. 2013;31(2):187–219. https://doi.org/10.1260/0144-5987.31.2.187.
Liu Y, Zhang JC, Ren J, et al. Stable isotope geochemistry of the nitrogen-rich gas from lower Cambrian shale in the Yangtze Gorges area, South China. Mar Pet Geol. 2016;77:693–702. https://doi.org/10.1016/j.marpetgeo.2016.07.020.
Liu Y, Tang X, Zhang JC, et al. Geochemical characteristics of the extremely high thermal maturity transitional shale gas in the Southern North China Basin (SNCB) and its differences with marine shale gas. Int J Coal Geol. 2018;194:33–44. https://doi.org/10.1016/j.coal.2018.05.005.
Michelsen N, Reshid M, Siebert C, et al. Isotopic and chemical composition of precipitation in Riyadh, Saudi Arabia. Chem Geol. 2015;413:51–62. https://doi.org/10.1016/j.chemgeo.2015.08.001.
Pashin JC, Kopaska-Merkel DC, Arnold AC, et al. Gigantic, gaseous mushwads in Cambrian shale: Conasauga Formation, southern Appalachians, USA. Int J Coal Geol. 2012;103:70–91. https://doi.org/10.1016/j.coal.2012.05.010.
Qu ZY. Shale gas generation and variation in stable carbon and hydrogen isotope compositions. Masters Dissertation, Guangzhou Institute of Geochemistry, University of Chinese Academy of Science, 2015 (**in Chinese**).
Qu ZY, Sun JN, Shi JT, et al. Characteristics of stable carbon isotopic composition of shale gas. Natl Gas Geosci. 2015;26(7):1376–84 **(in Chinese)**.
Rao S, Zhu CQ, Wang Q, et al. Thermal evolution patterns of the Sinian-Lower Paleozoic source rocks in the Sichuan basin, southwest China. Chin J Geophys. 2013;56(5):1549–59 **(in Chinese)**.
Tilley B, Muehlenbachs K. Isotope reversals and universal stages and trends of gas maturation in sealed, self-contained petroleum systems. Chem Geol. 2013;339:194–204. https://doi.org/10.1016/j.chemgeo.2012.08.002.
Wang Z. Characterization of the microscopic pore structure of the lower paleozoic shale gas reservoir in the Southern Sichuan Basin and its influence on gas content. Pet Sci Technol. 2017;35(23):2165–71. https://doi.org/10.1080/10916466.2017.1390682.
Wang Q, Li RR. Research status of shale gas: a review. Renew Sustain Energy Rev. 2017;74:715–20. https://doi.org/10.1016/j.rser.2017.03.007.
Wang XP, Mou CL, Wang QY, et al. Diagenesis of black shale in Longmaxi Formation, southern Sichuan Basin and its periphery. Acta Pet Sin. 2015;36(9):1035–47 **(in Chinese)**.
Wang Q, Zhang DY, Wang J, et al. Hydrocarbon and non-hydrocarbon characteristics for comprehensive identification about kerogen pyrolysis gas and oil cracked gas. Nat Gas Geosci. 2018;29(9):1231–9 **(in Chinese)**.
Wang Y, Wang LH, Wang JQ, et al. Multiscale characterization of three-dimensional pore structures in a shale gas reservoir: a case study of the Longmaxi shale in Sichuan basin, China. J Nat Gas Sci Eng. 2019;66:207–16. https://doi.org/10.1016/j.jngse.2019.04.009.
Wei GQ, Xie ZY, Song JR, et al. Features and origin of natural gas in the Sinian-Cambrian of central Sichuan paleo-uplift, Sichuan Basin, SW China. Pet Explor Dev. 2015;42(6):768–77. https://doi.org/10.1016/S1876-3804(15)30073-2.
Wellman RP, Cook FD, Krouse HR. Nitrogen-15: microbiological alteration of abundance. Science. 1968;161(3838):269–70. https://doi.org/10.1126/science.161.3838.269.
Whelan JK, Solomon PR, Desphande GV, et al. Thermogravimetric fourier transform infrared spectroscopy (TG-FTIR) of petroleum source rocks-Initial results. Energy Fuels. 1988;2:65–73. https://doi.org/10.1021/ef00007a010.
Wu P, Liu SF, Dou GX. Sedimentary response to Emeishan mantle plume in the eastern Yunnan Province. Acta Petrol Sin. 2014;30(6):1793–803 **(in Chinese)**.
Wu W, Fang CC, Dong DZ, et al. Shale gas geochemical anomalies and gas source identification. Acta Pet Sin. 2015;36(11):1332–40 **(in Chinese)**.
Wu J, Liang C, Jiang ZX, et al. Shale reservoir characterization and control factors on gas accumulation of the Lower Cambrian Niutitang shale, Sichuan Basin, South China. Geol J. 2018;54(3):1604–16. https://doi.org/10.1002/gj.3255.
Xia P, Wang GL, Zeng FG, et al. The characteristics and mechanism of high-over matured nitrogen-rich shale gas of Niutitang Formation, northern Guizhou area. Nat Gas Geosci. 2018;29(9):1345–55 **(in Chinese)**.
Xu YG, He B, Chung SL, et al. Geologic, geochemical and geophysical consequences of plume involvement in the Emeishan flood-basalt province. Geology. 2004;32(10):917–20. https://doi.org/10.1130/G20602.1.
Zhao JH, Jin ZJ, Jin ZK, et al. Lithofacies types and sedimentary environment of shale in Wufeng-Longmaxi Formation, Sichuan Basin. Acta Pet Sin. 2016;37(5):572–86 **(in Chinese)**.
Zhu YN, Shi BQ, Fang CB. The isotopic compositions of molecular nitrogen: implications on their origins in natural gas accumulations. Chem Geol. 2000;164(3–4):321–30. https://doi.org/10.1016/S0009-2541(99)00151-5.
Zhu CQ, Tian YT, Xu M, et al. The effect of Emeishan supper mantle plume to the thermal evolution of source rocks in the Sichuan basin. Chin J Geophys. 2010;53(1):119–27 **(in Chinese)**.
Zou CN, Dong DZ, Wang YM, et al. Shale gas in China: characteristics, challenges and prospects (II). Pet Explor Dev. 2016;43(2):182–96. https://doi.org/10.1016/S1876-3804(16)30022-2.
Zumberge J, Ferworn K, Brown S. Isotopic reversal ('rollover') in shale gases produced from the Mississippian Barnett and Fayetteville Formations. Mar Pet Geol. 2012;31(1):43–52. https://doi.org/10.1016/j.marpetgeo.2011.06.009.